

Quadratic momentum dependence in the nucleon-nucleon interaction

R. B. Wiringa[*]

Physics Division, Argonne National Laboratory, Argonne, IL 60439

A. Arriaga[†]

*Centro de Fisica Nuclear da Universidade de Lisboa,
Avenida Gama Pinto 2, 1699 Lisboa, Portugal
and Departamento de Fisica, Faculdade de Ciências
da Universidade de Lisboa, 1700 Lisboa, Portugal*

V. R. Pandharipande[‡]

*Department of Physics, University of Illinois at Urbana-Champaign,
1110 West Green Street, Urbana, IL 61801*

(Dated: November 14, 2018)

Abstract

We investigate different choices for the quadratic momentum dependence required in nucleon-nucleon potentials to fit phase shifts in high partial-waves. In the Argonne v_{18} potential \mathbf{L}^2 and $(\mathbf{L} \cdot \mathbf{S})^2$ operators are used to represent this dependence. The v_{18} potential is simple to use in many-body calculations since it has no quadratic momentum-dependent terms in S -waves. However, \mathbf{p}^2 rather than \mathbf{L}^2 dependence occurs naturally in meson-exchange models of nuclear forces. We construct an alternate version of the Argonne potential, designated Argonne v_{18pq} , in which the \mathbf{L}^2 and $(\mathbf{L} \cdot \mathbf{S})^2$ operators are replaced by \mathbf{p}^2 and Q_{ij} operators, respectively. The quadratic momentum-dependent terms are smaller in the v_{18pq} than in the v_{18} interaction. Results for the ground state binding energies of ^3H , ^3He , and ^4He , obtained with the variational Monte Carlo method, are presented for both the models with and without three-nucleon interactions. We find that the nuclear wave functions obtained with the v_{18pq} are slightly larger than those with v_{18} at interparticle distances < 1 fm. The two models provide essentially the same binding in the light nuclei, although the v_{18pq} gains less attraction when a fixed three-nucleon potential is added.

PACS numbers: PACS numbers: 13.75.Cs, 21.30.-x, 21.45.+v

I. INTRODUCTION

A number of choices have to be made in arriving at a form used to represent the nucleon-nucleon (NN) interaction by a model potential operator v_{ij} . In general, models with different choices will give different results for systems with three and more nucleons. When we add many-body forces to the Hamiltonian, they too depend upon the choice made for v_{ij} . In principle all realistic combinations of NN and three-nucleon ($3N$) interaction, V_{ijk} , should give identical results for the three-nucleon system by construction. We can similarly define combinations of 2-, 3-, 4- and many-nucleon interactions such that they give the same results for many-nucleon systems. However, such constructions are probably useful only when the contributions of n -body interactions decrease rapidly with n . In practice the contribution of realistic V_{ijk} is much smaller than that of v_{ij} , and the 4- and higher-nucleon terms in the Hamiltonian are often neglected.

All realistic models of NN interaction [1, 2, 3] have a one-pion-exchange (OPE) character at long range, which is absolutely essential to fit high partial-wave data. The choices to be made for the OPE interaction are well known. As emphasized by Friar [4, 5], they are related by unitary transformations which generate the appropriate pion-exchange terms in V_{ijk} . For example, a significant part of the difference between the Bonn potential [3] and the Nijmegen [1] and Argonne [2] potentials is due to the choice made for the OPE interaction [6].

In contrast, the origins of the shorter-range parts of the NN interaction are not well known, and the choices made to model those are more pragmatic. When the model is intended for use in many-body problems, the accuracy with which it reproduces two-body data and the ease with which it can be used in calculations are primary considerations [2]. Phenomenological three-body forces, determined from data [7], are used with these models. They should reduce the dependence of the calculated many-body observables on the choices made to represent v_{ij} .

Realistic models of the shorter-range parts of the NN interaction can be broadly categorized as phenomenological, meson-exchange, or based on effective field theory. Here we focus on phenomenological models which can accurately reproduce the two-nucleon data. The meson-exchange models contain phenomenological effective mesons, and in models such as the CD Bonn [3] their masses and couplings depend upon the NN partial wave. Most

models based on effective field theory do not yet fit the scattering data as well.

Phenomenological models use an operator construct, such as:

$$v_{ij} = \sum_{p=1,n} v_p(r_{ij}) O_{ij}^p . \quad (1)$$

They are based on the demonstration [8] that the most general form satisfying translational, rotational, parity, and time-reversal invariance can be written as:

$$\begin{aligned} v_{NN} = & v_c + v_\sigma \sigma_i \cdot \sigma_j + v_t S_{ij} + v_{ls} (\mathbf{L} \cdot \mathbf{S})_{ij} \\ & + v_{\sigma l} L_{ij} + v_{\sigma p} \sigma_i \cdot \mathbf{p} \sigma_j \cdot \mathbf{p} , \end{aligned} \quad (2)$$

with the tensor and quadratic spin-orbit operator definitions:

$$S_{ij} = 3 \sigma_i \cdot \hat{\mathbf{r}} \sigma_j \cdot \hat{\mathbf{r}} - \sigma_i \cdot \sigma_j \quad (3)$$

$$L_{ij} = \frac{1}{2} \{ \sigma_i \cdot \mathbf{L}, \sigma_j \cdot \mathbf{L} \} . \quad (4)$$

Fortunately, on-energy-shell data require only two of the three possible tensor operators, S_{ij} , L_{ij} , and $\sigma_i \cdot \mathbf{p} \sigma_j \cdot \mathbf{p}$. The last one has been omitted in all models [9] since the potential associated with it does not have a known theoretical motivation.

The individual v_x in Eq.(2) can be functions of r , \mathbf{p}^2 , or \mathbf{L}^2 , and can have a general isospin dependence:

$$\begin{aligned} v_x = & v_x^0(r, \mathbf{p}^2, \mathbf{L}^2) + v_x^\tau(r, \mathbf{p}^2, \mathbf{L}^2) \tau_i \cdot \tau_j \\ & + v_x^T(r, \mathbf{p}^2, \mathbf{L}^2) T_{ij} + v_x^{\tau z}(r, \mathbf{p}^2, \mathbf{L}^2) (\tau_{zi} + \tau_{zj}) , \end{aligned} \quad (5)$$

where the first two terms are charge-independent (CI), the next has the charge-dependent (CD) isotensor operator $T_{ij} = 3\tau_{zi}\tau_{zj} - \tau_i \cdot \tau_j$, and the last is a charge-symmetry-breaking (CSB) isovector component. The nuclear CD and CSB forces are much smaller than the CI terms.

All modern NN potentials formulated in an operator structure contain the eight basic CI operators arising from the first line of Eq.(2):

$$O_{ij}^{p=1,8} = [1, \sigma_i \cdot \sigma_j, S_{ij}, \mathbf{L} \cdot \mathbf{S}] \otimes [1, \tau_i \cdot \tau_j] . \quad (6)$$

These eight operators are sufficient to fit a CI average of S - and P -waves and to obtain good deuteron properties. Any interaction that is static or has linear terms in momentum can

be represented as a sum of these eight operators. Typically six additional operator terms that are quadratic in either angular or linear momentum are required to fit higher partial waves. For example, the Urbana v_{14} [10] and Argonne v_{14} [11] potentials use the additional operators:

$$O_{ij}^{p=9,14} = [\mathbf{L}^2, (\sigma_i \cdot \sigma_j) \mathbf{L}^2, (\mathbf{L} \cdot \mathbf{S})^2] \otimes [1, \tau_i \cdot \tau_j] , \quad (7)$$

where $(\mathbf{L} \cdot \mathbf{S})^2$ is simply related to L_{ij} :

$$L_{ij} = \mathbf{L} \cdot \mathbf{S} - \mathbf{L}^2 + 2(\mathbf{L} \cdot \mathbf{S})^2 . \quad (8)$$

The more modern Argonne v_{18} (AV18) potential of Ref. [2] (hereafter referred to as WSS) supplements these fourteen CI operators with four small CD and CSB terms and a complete electromagnetic interaction.

The Super-Soft-Core (SSC) potential [12] also used four \mathbf{L}^2 operators, but with the angular momentum tensor operator Q_{ij}

$$Q_{ij} = 3L_{ij} - (\sigma_i \cdot \sigma_j) \mathbf{L}^2 , \quad (9)$$

or, in a later version [9], the L_{ij} operator as the specific quadratic spin-orbit term. The Q_{ij} and $(\mathbf{L} \cdot \mathbf{S})^2$ operators vanish in $S = 0$ states, while the L_{ij} does not. Still other variations of the quadratic spin-orbit operator, related via Eqs.(8) and (9), have been used in the past.

The Urbana, Argonne, and SSC models are all local potentials in each NN partial wave denoted by quantum numbers L, S, J . In single channels having $L = J$, the v_{LSJ} is a central function of r , while in coupled channels having $L = J \pm 1$, the v_{LSJ} is a sum of central, tensor and spin-orbit interactions. In contrast, the parametrized Paris potential [13] was constructed with \mathbf{p}^2 operators instead of \mathbf{L}^2 , i.e.,

$$v(r, \mathbf{p}^2) = v^c(r) + \mathbf{p}^2 v^{p2}(r) + v^{p2}(r) \mathbf{p}^2 , \quad (10)$$

with

$$\mathbf{p}^2 = - \left[\frac{1}{r} \frac{d^2}{dr^2} r - \frac{\mathbf{L}^2}{r^2} \right] , \quad (11)$$

where we have set $\hbar = 1$ for brevity. Because \mathbf{p}^2 does not commute with functions of r , a momentum-dependent potential like Paris can be more difficult to use in many-body calculations, especially configuration-space methods such as quantum Monte Carlo [14] and variational methods using chain summation techniques. In fact the Urbana model with \mathbf{L}^2

and $(\mathbf{L} \cdot \mathbf{S})^2$ operators was proposed to avoid difficulties encountered in variational calculations of nucleon matter with the Paris potential [15]. On the other hand, \mathbf{p}^2 operators are more likely to arise in field-theoretic models for the NN interaction.

In 1993 the Nijmegen group [16] produced a multienergy partial-wave analysis of elastic NN data below $T_{lab} = 350$ MeV (PWA93) that was able to reproduce over 4300 data points with a $\chi^2/\text{datum} \sim 1$. This was followed by a series of comparably accurate potential models, including their own Nijm I, Nijm II, and Reid93 potentials [1], AV18 [2], and CD Bonn [3]. All these models use an operator construct in some fashion, with the Nijm II, Reid93, and AV18 choosing operators which give local potentials in each partial wave, while Nijm I includes \mathbf{p}^2 terms and CD Bonn has additional momentum-dependent terms. However, with the exception of AV18, they are all adjusted partial-wave by partial-wave. The isoscalar v_{14} part of the v_{18} potentials contains only five independent interactions in $S = 1$ states and two in $S = 0$ states, *i.e.*, seven each for the two isospin values $T = 0$ and 1. In the $S = 1$ states they correspond to the central, tensor, spin-orbit, \mathbf{L}^2 or \mathbf{p}^2 , and $(\mathbf{L} \cdot \mathbf{S})^2$ or Q_{ij} , while in the $S = 0$ states we have only the central and \mathbf{L}^2 or \mathbf{p}^2 potentials. In the $T = 1$, $S = 1$ states, for example, the five potentials can be extracted from the interactions in the 3P_0 , 3P_1 and ${}^3P_2 - {}^3F_2$ partial waves. The isoscalar interactions in all the 3F_3 and higher $T = 1$, $S = 1$ partial waves are related to those in the 3P_0 , 3P_1 and ${}^3P_2 - {}^3F_2$ in a v_{18} model. Similar relations exist in partial waves with $S = 0$. However, these relations are lost when the meson coupling constants or masses are varied to fit each partial wave, and have different values in each partial wave, as in the Nijmegen and Bonn models. These potentials therefore have additional nonlocalities which are best represented with partial-wave projection operators.

Calculations of trinucleon and alpha binding energies with the five potentials mentioned above indicate that the three partial-wave local potentials give similar results, but the other two give more binding [17, 18]. CD-Bonn gives 0.4 and 2.0 MeV more binding than AV18 in ${}^3\text{H}$ and ${}^4\text{He}$, but a large part of it could be due to nonlocal representation of the OPE potential used in that model. As mentioned earlier, this extra binding goes into the three-nucleon interactions used with the other models. Nijm I uses the local OPE potential, but has shorter-range momentum-dependent terms. It gives only 0.1 and 0.7 MeV more binding. However, none of the models is able to reproduce the experimental binding energies without the addition of a three-nucleon potential.

The purpose of this paper is to study the practical consequences of using \mathbf{p}^2 instead of

\mathbf{L}^2 operators in potential models. To do this, we construct a variant of the AV18 potential, using the same spatial functions and refitting the adjustable parameters to make the model as phase equivalent to AV18 as possible. As discussed below, our best reproduction of AV18 phases also involves changing the quadratic spin-orbit operator from $(\mathbf{L} \cdot \mathbf{S})^2$ to Q_{ij} . As a result, we designate this new model as Argonne v_{18pq} (AV18pq) to denote the two changes in operator structure, $\mathbf{L}^2 \rightarrow \mathbf{p}^2$ and $(\mathbf{L} \cdot \mathbf{S})^2 \rightarrow Q_{ij}$.

In Sec. II we describe the construction of the new potential and present a comparison of phase shifts and radial forms with respect to AV18. In Sec. III we present variational Monte Carlo calculations of the $A = 3, 4$ nuclei for both models, and with different three-nucleon potentials added. Our conclusions are given in Sec. IV.

II. POTENTIAL CONSTRUCTION

The practical need for the quadratic momentum-dependent operators is to simultaneously fit the phase shifts in S - and D -waves and in P - and F -waves. For example, a static potential with components of one- and two-pion exchange ranges and a shorter-range core cannot fit the 1S_0 and 1D_2 phase shifts. The \mathbf{L}^2 dependent term in the v_{18} interaction operator generates a difference between the potentials in 1S_0 and 1D_2 waves, and allows one to fit the phase shifts very accurately.

Quadratic spin-orbit terms are necessary for fitting the variety of data in higher $S = 1$ partial waves, such as $^3D_{1,2,3}$ and $^3F_{2,3,4}$. The AV18 is written with $(\mathbf{L} \cdot \mathbf{S})^2$ operators, but it can be algebraically recast with either the L_{ij} or Q_{ij} operators, with reshuffling of contributions among the $(\mathbf{L} \cdot \mathbf{S})^2$, $\mathbf{L} \cdot \mathbf{S}$ and \mathbf{L}^2 terms. As discussed below, we find it expedient to choose the Q_{ij} operator, so we use AV18 in this representation, which we designate as AV18q for clarity. This will allow us to study the difference between choosing \mathbf{p}^2 or \mathbf{L}^2 keeping all other operators the same. This recast potential is the same as AV18, but its \mathbf{L}^2 and $\mathbf{L} \cdot \mathbf{S}$ terms contain parts of the $(\mathbf{L} \cdot \mathbf{S})^2$ terms via Eqs. (8) and (9).

Inserting Eq.(11) in Eq.(10) we get

$$v(r, p^2) = v^c(r) - \left\{ \frac{1}{r} \frac{d^2}{dr^2} r, v^{p2}(r) \right\} + 2v^{p2}(r) \frac{L^2}{r^2}. \quad (12)$$

Therefore, in order to make comparison of terms in AV18q and AV18pq meaningful we

define:

$$v_{ST}^{p2}(r) = \frac{1}{2}r^2 v_{ST}^{l2}(r) . \quad (13)$$

The \mathbf{L}^2 term in AV18pq then has the same form as that in AV18q. Formally any v_{18pq} model is obtained by adding the radial derivatives in \mathbf{p}^2 , as given in Eq.(11), to a \tilde{v}_{18q} potential:

$$v_{18pq} = \tilde{v}_{18q} - \left\{ \frac{1}{r} \frac{d^2}{dr^2} r, \frac{1}{2} r^2 v^{l2} \right\} . \quad (14)$$

However, the parameters of \tilde{v}_{18q} are not equal to those of v_{18q} which fits the phase shifts without the term with radial derivatives.

The intermediate- and short-range parts of AV18pq are parameterized as in AV18 or equivalently AV18q. They are given by:

$$\begin{aligned} v_{ST}^x(r) &= v_{ST}^\pi + I_{ST}^x T_\mu^2(r) \\ &+ \left[P_{ST}^x + \mu r Q_{ST}^x + (\mu r)^2 R_{ST}^x \right] W(r) . \end{aligned} \quad (15)$$

Here x can be c , t , ls , $l2$ or q for the central, tensor, spin-orbit, either \mathbf{L}^2 or \mathbf{p}^2 , and Q_{ij} interactions. The v_{ST}^π denotes the OPE interaction which contributes to terms with $x = c$ and t . The average pion mass is μ , $T_\mu(r)$ is the tensor Yukawa function (with a cutoff), and the shape of the intermediate-range interaction is approximated with $T_\mu^2(r)$. A Woods-Saxon function $W(r)$ is used to parametrize the short-range part.

The radial wave equation for $u(r)/r$ in single channels with the AV18q potential is

$$\frac{1}{2M_r} u''(r) = \left(\frac{1}{2M_r} \frac{\ell(\ell+1)}{r^2} + v_{ch}(r) - E \right) u(r) , \quad (16)$$

where $v_{ch}(r)$ is the potential in that channel given by the v_{18q} operator. We solve this equation numerically using the Numerov method, which is particularly efficient for second-order differential equations without first derivative terms. With the addition of the derivative terms of Eq.(14), the radial wave equation for AV18pq generalizes to

$$\begin{aligned} &\left(\frac{1}{2M_r} + 2v_{ST}^{p2}(r) \right) u''(r) + 2[v_{ST}^{p2}(r)]' u'(r) \\ &= \left(\frac{1}{2M_r} \frac{\ell(\ell+1)}{r^2} + \tilde{v}_{ch}(r) - [v_{ST}^{p2}(r)]'' - E \right) u(r) . \end{aligned} \quad (17)$$

Although this expression has a first derivative of the wave function in it, it can be solved by the Numerov method with a simple substitution:

$$w(r) = \xi(r) u(r) = [1 + 4M_r v_{ST}^{p2}(r)]^{1/2} u(r) . \quad (18)$$

Then Eq.(17) can be rewritten as

$$D(r)w''(r) = \eta(r)w(r) , \quad (19)$$

with the definitions

$$D(r) = \frac{1}{2M_r} + 2v_{ST}^{p2}(r) , \quad (20)$$

$$\eta(r) = \frac{1}{2M_r} \frac{\ell(\ell+1)}{r^2} + \tilde{v}_{ch}(r) - \frac{([v_{ST}^{p2}(r)]')^2}{D(r)} - E . \quad (21)$$

The above method is easily generalized for the coupled channels, because the new terms of the potential do not couple channels. In all other respects, the AV18pq potential is constructed with the same form as AV18q. The same set of fundamental constants is used. The long-range electromagnetic and one-pion-exchange terms are identical, including their short-range cutoffs. The strength parameters, I_{ST}^x , P_{ST}^x , Q_{ST}^x , and R_{ST}^x are refit to make AV18pq as phase equivalent as possible to AV18 \equiv AV18q. Note that the parameters $P_{ST}^{x=t}$ and $Q_{ST}^{x\neq t}$, are determined from the required behavior of $v^x(r \rightarrow 0)$, as discussed by WSS.

The choice of Q_{ij} as the quadratic spin-orbit operator allows us to fit the $S = 0$ and $S = 1$ phases for given T separately. The $J \leq 4$ phases are fit for eleven different energies, in the range 1 – 350 MeV, as well as scattering lengths and deuteron binding. In the $T = 1$ phases, we want the quadratic momentum-dependent parts of the potential to be charge-independent, so we determine them first by fitting the phases produced by the CI part of the AV18 potential, including the CI average of one-pion exchange. Once these parts are fixed, we adjust the central part of the $S = 0$ potential separately for pp and np phases, including full charge-dependence in OPE; this sets the CD parts of the interaction. The nn potential is then slightly altered from the pp potential to reproduce the nn scattering length, which is the only constraint on strong charge-symmetry breaking. The CSB in $ST = 11$ channels is adjusted, as for AV18, such that the final potential in operator projection has no spin-dependent CSB, aside from electromagnetic terms. Fitting the $T = 0$ channels is straightforward, including reproduction of the deuteron properties.

The adjusted parameter values for AV18pq are given in Table I, in which lines labeled $l2$ give the coefficients of the v_{ST}^{l2} related to v_{ST}^{p2} by Eq.(13). The rms deviations in degrees of the AV18pq phases from AV18 phases are given in Table II for pp scattering, and in Table III for np . These are binned over three different energy ranges, and in total. To help judge the

size of these errors, in the last column we quote the phase shift errors of PWA93 summed in a similar fashion.

It is apparent from the table that the $S = 0$ phases have been reproduced very well, with rms deviations much smaller than the experimental uncertainty. The $S = 1$ phases are more difficult to reproduce, although the rms deviations remain generally quite small. The places where they exceed the PWA93 errors are in the 3P_2 , 3F_4 , and higher $T = 1$ phases, and in the 3S_1 , 3D_3 , and 3G_4 $T = 0$ phases. The deviations are concentrated at the higher energies.

We also attempted fits using either $(\mathbf{L} \cdot \mathbf{S})^2$ or L_{ij} as alternate quadratic spin-orbit operators. Since $(\mathbf{L} \cdot \mathbf{S})^2$ vanishes in $S = 0$ states, the potential in these channels is the same as in AV18pq. For the $ST = 11$ phases, we were able to get a slightly better reproduction of the AV18 model, including 3P_2 and 3F_4 deviations that fall below the PWA93 errors. However, the $ST = 10$ phases were notably worse, with 3D_1 , 3D_2 , and 3G_4 phases having total rms deviations ~ 0.3 degrees, which we judge to be unacceptable. To use L_{ij} , we must fit $S = 0, 1$ channels simultaneously for given T , since this operator does not vanish in $S = 0$. We were able to get an even better reproduction of the AV18 $T = 0$ phases with this operator, but we could not find acceptable $T = 1$ solutions. This does not mean that good \mathbf{p}^2 potentials cannot be made with the L_{ij} or $(\mathbf{L} \cdot \mathbf{S})^2$ quadratic spin-orbit operators, but only that they may not work so well with the radial functions of the AV18 model.

We now compare the AV18q and AV18pq interactions with each other and with the AV8' interaction which has no quadratic momentum-dependent terms. It has only the eight leading operators of Eq.(6) plus Coulomb interaction between protons; it exactly reproduces the AV18 potential in 1S_0 , ${}^3S_1 - {}^3D_1$ and all the P -waves, except for the small CD and CSB terms and non-Coulombic electromagnetic terms. The AV8' is obtained from the AV18 by a simple reprojection of the operators [19], and is not phase equivalent to AV18 and AV18pq in D - and higher waves. Recall that AV18q is obtained by recasting AV18 with the identity:

$$(\mathbf{L} \cdot \mathbf{S})^2 = \frac{1}{2} \left(1 + \frac{1}{3} \sigma_1 \cdot \sigma_j \right) \mathbf{L}^2 - \frac{1}{2} \mathbf{L} \cdot \mathbf{S} + \frac{1}{6} Q_{ij} , \quad (22)$$

and that the only difference between the operator structure of AV18q and AV18pq is $\mathbf{L}^2 \rightarrow \mathbf{p}^2$.

The central potentials in $ST = 01$ and 10 channels are compared in Fig. 1. In these spin-isospin channels the v_{ST}^c are those in the S and higher even waves, and they are the same in AV18q and AV8' models. The $ST = 01$ and 10 central potentials in AV18pq have

a slightly smaller repulsive core. This is to be expected. The \mathbf{L}^2 and Q_{ij} operators are zero in S -waves. In the AV18q and AV8' models the change in the sign of S -wave phases at higher energies is produced by the repulsive core in the interaction. In contrast the \mathbf{p}^2 part of AV18pq operates in the S -waves also. It becomes more repulsive at larger energies, and helps turn the S -wave phase shifts negative together with the repulsive core.

The v_{ST}^c in $ST = 00$ and 11 states are compared in Fig. 2; they occur in P - and higher odd waves. In these states the AV8' has a larger repulsive core than either AV18 or AV18pq. The odd partial wave v^c in AV8' contain the contribution of \mathbf{L}^2 and Q_{ij} operators in P -waves. The repulsive cores in these states are obviously more sensitive to the treatment of quadratic momentum dependence as seen by comparing the AV18q and AV18pq curves. They are comparable to the centrifugal barrier, $2/(Mr^2)$, in P -waves. For example, the centrifugal barrier is ~ 330 MeV at $r = 0.5$ fm. Fortunately nuclear energies are not very sensitive to the repulsive cores in P - and higher waves.

The $r^2 v_{ST}^{l2}$ are compared in Figs. 3 and 4. Recall that the $v^{p2} = r^2 v^{l2}/2$, and that \mathbf{L}^2 also contains a r^2 factor. Therefore $r^2 v_{ST}^{l2}(r)$ are the relevant functions. In all cases the \mathbf{p}^2 dependent terms in AV18pq are smaller than the corresponding \mathbf{L}^2 terms in AV18q. The Q_{ij} potentials are also smaller in AV18pq as shown in Fig. 5.

The tensor and spin-orbit potentials are compared in Figs. 6 and 7. The tensor potentials are weaker in AV8' but similar in AV18q and AV18pq. The large spin-orbit potential in $ST = 11$ states is similar in all the models. However, the smaller spin-orbit potential in $ST = 01$ channel is relatively much weaker in AV18pq.

The potentials in ST states can be cast into an operator format using $\sigma_i \cdot \sigma_j$ and $\tau_i \cdot \tau_j$ operators as detailed in Sec. IV of WSS. The v_{ST}^c recast as the sum:

$$v_c(r) + v_\tau(r) \tau_i \cdot \tau_j + v_\sigma(r) \sigma_i \cdot \sigma_j + v_{\sigma\tau}(r) \tau_i \cdot \tau_j \sigma_i \cdot \sigma_j \quad (23)$$

are shown in Fig. 8. At small r , where v_c dominates, the smaller v_τ , v_σ and $v_{\sigma\tau}$ are poorly determined by the data. The pair current operators depend upon these components of the interaction. For example, in Riska's method [20] the isovector, pseudoscalar and vector currents are obtained from the $v_{\sigma\tau}$ and $v_{\tau\tau}$ potentials associated with the $\sigma_i \cdot \sigma_j \tau_i \cdot \tau_j$ and $S_{ij} \tau_i \cdot \tau_j$ operators. In particular the v_σ and v_τ are very different in the AV18pq and AV18q models.

The deuteron properties of AV18q and AV18pq are compared in Table IV, along with the

expectation values of different components of the potential. The binding energy and other observables are virtually identical. The total kinetic and potential energies obtained with AV18pq are smaller by $\sim 1\%$. The net contribution of quadratic momentum-dependent terms in AV18pq, $\langle v^p{}^2 + v^q \rangle = 0.086$ MeV, is noticeably smaller than the $\langle v^{l2} + v^q \rangle = -0.331$ MeV for AV18q.

The deuteron wave functions, $u(r)$ and $w(r)$, are illustrated in Fig. 9; the AV18pq functions peak at slightly smaller values of r . Impulse calculations of the deuteron structure function $A(q^2)$ are virtually identical, but the $B(q^2)$ structure function has its minimum pushed to larger momenta, and likewise the zero crossing of the tensor polarization $T_{20}(q^2)$ also increases. However, consistent two-body current contributions constructed for AV18pq should be added before the electromagnetic observables are compared in detail with AV18 predictions or experiment.

III. LIGHT NUCLEI CALCULATIONS

We have used variational Monte Carlo (VMC) techniques to calculate and compare the effect of AV8', AV18=AV18q, and AV18pq potentials on the binding of $A = 3, 4$ light nuclei. AV8' has been used in a benchmark study of four-nucleon binding [21] and is the interaction used for propagation in Green's function Monte Carlo (GFMC) calculations. Finally, we study the effects of adding an explicit three-nucleon potential to the Hamiltonian, either Urbana IX (UIX) [22] or the TM' variant [23] of the Tucson-Melbourne force [24]. (We use TM' with the cutoff $\Lambda = 4.756m_\pi$ as determined in Ref. [18] to be appropriate for use with AV18.)

The VMC calculations are described in Refs. [25, 26]. We use the trial wave function

$$|\Psi_V\rangle = \left[1 + \sum_{i < j < k} (U_{ijk} + U_{ijk}^{TNI}) \right] |\Psi_P\rangle , \quad (24)$$

where the pair wave function, Ψ_P , is given by

$$|\Psi_P\rangle = \left[\mathcal{S} \prod_{i < j} (1 + U_{ij}) \right] |\Psi_J\rangle . \quad (25)$$

The U_{ij} , U_{ijk} , and U_{ijk}^{TNI} are noncommuting two- and three-nucleon correlation operators, and \mathcal{S} is a symmetrization operator. The antisymmetric Jastrow wave function, Ψ_J , depends

on the state under investigation, but for S-shell nuclei takes the simple form:

$$|\Psi_J\rangle = \left[\prod_{i < j < k} f_{ijk}^c(\mathbf{r}_{ik}, \mathbf{r}_{jk}) \prod_{i < j} f_c(r_{ij}) \right] |\Phi_A(JMTT_3)\rangle . \quad (26)$$

The $f_c(r_{ij})$ and f_{ijk}^c are central (spin-isospin independent) two- and three-body correlation functions and Φ_A is an antisymmetric spin-isospin state,

$$|\Phi_3(\frac{1}{2}\frac{1}{2}\frac{1}{2}\frac{1}{2})\rangle = \mathcal{A}|\uparrow p \downarrow p \uparrow n\rangle , \quad (27)$$

$$|\Phi_4(0000)\rangle = \mathcal{A}|\uparrow p \downarrow p \uparrow n \downarrow n\rangle , \quad (28)$$

with \mathcal{A} the antisymmetrization operator.

The two-body correlation operator U_{ij} is a sum of spin, isospin, and tensor terms:

$$U_{ij} = \sum_{p=2,6} \left[\prod_{k \neq i,j} f_{ijk}^p(\mathbf{r}_{ik}, \mathbf{r}_{jk}) \right] u_p(r_{ij}) O_{ij}^p , \quad (29)$$

where the O_{ij}^p are the first six operators of Eq.(6). The f_{ijk}^p is another central three-body correlation function. In previous calculations we also introduced a spin-orbit correlation in the sum of Eq.(24), but it is expensive to calculate and improves the binding energy only a little; we neglect such correlations here.

The central $f_c(r)$ and noncentral $u_p(r)$ pair correlation functions reflect the influence of the two-body potential at short distances, while satisfying asymptotic boundary conditions of cluster separability. Reasonable functions are generated by minimizing the two-body cluster energy of a somewhat modified NN interaction; this results in a set of coupled, Schrödinger-like, differential equations corresponding to linear combinations of the operators in v_{ij} , with a number of embedded variational parameters [25].

For the AV18pq potential, these differential equations must be generalized to take into account the influence of the v^{p2} terms. However, by studying the changes in the Schrödinger equation for the phase shifts, Eqs.(16-21) above, we find three simple substitutions that generalize the correlation generators, Eqs.(2.2-2.5) of Ref. [25], to produce the appropriate correlation functions f_{ST} :

$$\begin{aligned} \frac{1}{2M_r} &\rightarrow D(r) , \\ v_{ch}(r) &\rightarrow \tilde{v}_{ch}(r) - \frac{([v_{ST}^{p2}(r)]')^2}{D(r)} , \\ f_{ST}(r) &\rightarrow f_{ST}(r)/\xi(r) . \end{aligned}$$

A reprojection of the $f_{ST}(r)$ into operator terms then yields the $f_c(r)$ and $u_p(r)$.

The f_{ijk}^c , f_{ijk}^p , and U_{ijk} are three-nucleon correlations also induced by v_{ij} ; details may be found in Ref. [26]. The U_{ijk}^{TNI} are three-body correlations induced by the three-nucleon interaction, which have the form suggested by perturbation theory:

$$U_{ijk}^{TNI} = \sum_x \epsilon_x V_{ijk}(\tilde{r}_{ij}, \tilde{r}_{jk}, \tilde{r}_{ki}) , \quad (30)$$

with $\tilde{r} = yr$, y a scaling parameter, and ϵ_x a (small negative) strength parameter.

Results of our VMC calculations are given in Table V. We also show GFMC [7] and Faddeev-Yakubovsky (FY) [18] results for comparison, where available. The VMC results are typically 1.5–3% above the more exact GFMC and FY results, which agree with each other to better than 1%. The primary goal here is to judge the relative binding of the different Hamiltonians, and we think the VMC calculations are adequate for this purpose.

In all cases we see that the AV8', with no quadratic momentum dependence, gives the most binding. Both AV18 and AV18pq give less binding and the difference between their results is smaller than that from AV8'. From the point of view of fitting NN data, adding quadratic momentum-dependent terms to v_{ij} is the most important step, whether they be \mathbf{p}^2 or \mathbf{L}^2 . In $A=3$ and 4 nuclei these terms reduce the binding by ~ 2.5 and 4 % respectively. In the absence of three-nucleon interactions the reductions are nearly the same for AV18 and AV18pq. (In examining the $A = 3$ results, it is important to remember that aside from Coulomb interaction, AV8' is a charge-independent potential, so averages of the ^3H and ^3He energies show the differences more clearly.)

When a three-nucleon interaction is added to the Hamiltonian, as required to fit the experimental binding of light nuclei, the effect of adding quadratic momentum dependence grows to ~ 3 and 5 % for $A=3$ and 4 if AV18 is used, while a slightly larger effect of ~ 4 and 6 % is obtained with AV18pq. In practice the strengths of the various terms in the three-nucleon interaction are not known *a priori*. The short-range terms of this interaction depend upon the representation of v_{ij} , and can be different for AV18 and AV18pq. They should be chosen separately such that both models give the same, experimental trinucleon energy.

We note that this interplay between two- and three-nucleon interactions was already apparent in the Bochum FY calculations [18] for the Nijmegen potentials [1]. These results are also shown at the bottom of Table V. The nonlocal Nijm I potential gives slightly more

binding than the local Nijm II, but to obtain the experimental binding by adding a $3N$ force, a stronger version (larger $\Lambda \rightarrow$ weaker cutoff) is required to accompany the nonlocal NN potential, in this case chosen to reproduce the binding of ${}^3\text{He}$.

IV. CONCLUSIONS

We have constructed an AV18pq two-nucleon interaction that is essentially phase equivalent to AV18. The difference between the two interaction operators is the choice made for quadratic momentum-dependent terms. The AV18pq uses the \mathbf{p}^2 operator instead of the \mathbf{L}^2 used in AV18. The results obtained with these two interaction models for the $A = 2, 3$, and 4 bound states are compared with those of the AV8' model which has no quadratic momentum dependence.

The differences in the predicted deuteron wave functions are shown in Fig. 9. Those in the ${}^4\text{He}$ wave function can be judged from differences in the dominant central correlations in $ST = 01$, and central and tensor correlations in $ST = 10$ states shown in Fig. 10. In all these the magnitude of the wave function predicted by AV18pq is larger than that of AV18 or AV8' at small interparticle distance r . This is due to the smaller repulsive cores in the S -waves of AV18pq shown in Fig. 1.

In principle the deuteron form factors predicted by AV18pq will be different from those of AV18. We plan to calculate the current operators for AV18pq following the methods used for AV18 [2], and compare the predicted form factors with available data. Such a comparison could indicate if one of the two choices is more realistic.

The quadratic momentum-dependent terms give a small positive contribution to the ground-state energies of nuclei as can be seen from Table V. This contribution can depend upon the choice of interaction operators. In the absence of a $3N$ interaction, the quadratic momentum-dependent terms in AV18 and AV18pq give almost identical corrections, within 0.5%. However, a larger difference between AV18 and AV18pq develops when a fixed realistic $3N$ interaction is added to the nuclear Hamiltonian to obtain binding energies closer to the experimental values. In this case, the non-local AV18pq becomes less attractive than the local AV18, by $\sim 1\%$, just as the non-local Nijm I became relatively less attractive compared to the local Nijm II potential. One can presumably choose the parameters of the V_{ijk} to reproduce binding energies of nuclei with either AV18 or AV18pq.

All one-boson exchange models of nuclear forces give interactions with a \mathbf{p}^2 dependence. Electromagnetic and color forces also have a \mathbf{p}^2 dependence. On the other hand, nucleons are composite objects with internal excitations, and their interactions can have either \mathbf{L}^2 or \mathbf{p}^2 terms or both. The main motivation behind the choice of \mathbf{L}^2 was to simplify many-body calculations [15]. Green's function Monte Carlo methods can be used to study nuclei having $A \leq 12$ with AV8' type interactions that contain the dominant features of nuclear forces, but not the quadratic momentum dependence.

In GFMC studies with the AV18 interaction, the quadratic momentum-dependent terms are treated as a first-order perturbation [7]. The error δE in this calculation is given by:

$$\delta E = \langle \Psi_{18} | H_{18} | \Psi_{18} \rangle - \langle \Psi_{8'} | H_{18} | \Psi_{8'} \rangle , \quad (31)$$

where $|\Psi_{18}\rangle$ and $|\Psi_{8'}\rangle$ are the eigenstates obtained with the Hamiltonian H_{18} having the AV18 interaction and with $H_{8'}$ having the AV8' respectively. The Hamiltonians can include any static 3N interaction. The values obtained for δE in ${}^4\text{He}$, using optimum variational wave functions to approximate the $|\Psi_{18}\rangle$ and $|\Psi_{8'}\rangle$ are respectively 0.05, 0.16 and 0.03 MeV for AV18 alone and with UIX and TM' models of 3N interaction. They are less than 1% of the total energy.

A similar study using AV18pq instead of AV18 gives much larger estimates of 1.6, 1.1 and 1.8 MeV for the δE in the above three cases. These larger values are due to differences in the wave functions of AV8' and AV18pq models at small r (see Figs. 9 and 10). A first-order treatment of the difference between AV18pq and AV8' gives much too large an effect. It will be necessary to develop new techniques to perform accurate GFMC many-body calculations with the AV18pq interaction.

For those who wish to use the AV18pq potential model in their own applications, a FORTRAN subroutine is available online [27].

We thank S. C. Pieper for useful discussions. This work is supported by the U. S. Department of Energy, Nuclear Physics Division, under contract No. W-31-109-ENG-38, and the U. S. National Science Foundation via Grant No. PHY 00-98353.

- [*] Electronic address: wiringa@anl.gov
- [†] Electronic address: arriaga@ciifc.ul.pt
- [‡] Electronic address: vrp@uiuc.edu
- [1] V. G. J. Stoks, R. A. M. Klomp, C. P. F. Terheggen, and J. J. de Swart, Phys. Rev. C **49**, 2950 (1994).
- [2] R. B. Wiringa, V. G. J. Stoks, and R. Schiavilla, Phys. Rev. C **51**, 38 (1995).
- [3] R. Machleidt, F. Sammarruca, and Y. Song, Phys. Rev. C **53**, R1483 (1996); R. Machleidt, Phys. Rev. C **63**, 024001 (2001).
- [4] J. L. Friar, Ann. Phys. (N.Y.) **104**, 380 (1977).
- [5] S. A. Coon and J. L. Friar, Phys. Rev. C **34**, 1060 (1986).
- [6] J. L. Forest, Phys. Rev. C **61**, 034007 (2000).
- [7] S. C. Pieper, V. R. Pandharipande, R. B. Wiringa, and J. Carlson, Phys. Rev. C **64**, 014001 (2001).
- [8] S. Okubo and R. E. Marshak, Ann. Phys. (NY) **4**, 166 (1958).
- [9] R. de Tourreil, B. Rouben, and D. W. L. Sprung, Nucl. Phys. **A242**, 445 (1975).
- [10] I. E. Lagaris and V. R. Pandharipande, Nucl. Phys. **A359**, 331 (1981).
- [11] R. B. Wiringa, R. A. Smith, and T. L. Ainsworth, Phys. Rev. C **29**, 1207 (1984).
- [12] R. de Tourreil and D. W. L. Sprung, Nucl. Phys. **A201**, 193 (1973).
- [13] M. Lacombe, B. Loiseau, J. M. Richard, R. Vinh Mau, J. Côté, P. Pirès, and R. de Tourreil, Phys. Rev. C **21**, 861 (1980).
- [14] S. C. Pieper and R. B. Wiringa, Annu. Rev. Nucl. Part. Sci. **51**, 53 (2001).
- [15] I. E. Lagaris and V. R. Pandharipande, Nucl. Phys. **A359**, 349 (1981).
- [16] V. G. J. Stoks, R. A. M. Klomp, M. C. M. Rentmeester, and J. J. de Swart, Phys. Rev. C **48**, 792 (1993).
- [17] J. L. Friar, G. L. Payne, V. G. J. Stoks, and J. J. de Swart, Phys. Lett. B **311**, 4 (1993).
- [18] A. Nogga, H. Kamada, W. Glöckle, Phys. Rev. Lett. **85**, 944 (2000).

- [19] B. S. Pudliner, V. R. Pandharipande, J. Carlson, S. C. Pieper, and R. B. Wiringa, Phys. Rev. C **56**, 1720 (1997).
- [20] R. Schiavilla, V. R. Pandharipande and D. O. Riska, Phys. Rev. C **40**, 2294 (1989).
- [21] H. Kamada, *et al.* Phys. Rev. C **64**, 044001 (2001).
- [22] B. S. Pudliner, V. R. Pandharipande, J. Carlson, and R. B. Wiringa, Phys. Rev. Lett. **74**, 4396 (1995).
- [23] J. L. Friar, D. Hüber, U. van Kolck, Phys. Rev. C **59**, 53 (1999).
- [24] S. A. Coon, M. D. Scadron, P. C. McNamee, B. R. Barrett, D. W. E. Blatt, and B. H. J. McKellar, Nucl. Phys. **A317**, 242 (1979).
- [25] R. B. Wiringa, Phys. Rev. C **43**, 1585 (1991).
- [26] A. Arriaga, V. R. Pandharipande, and R. B. Wiringa, Phys. Rev. C **52**, 2362 (1995).
- [27] www.phy.anl.gov/theory/fewbody/av18pq.f

TABLE I: Short-range potential parameters in MeV. The asterisk denotes that the value was computed by Eq. (24) of WSS and not fit. The three shape parameters are: $c = 2.1 \text{ fm}^{-2}$, $r_0 = 0.5 \text{ fm}$, and $a = 0.2 \text{ fm}$.

Channel	Type	<i>I</i>	<i>P</i>	<i>Q</i>	<i>R</i>
$S = 0, T = 1(pp)$	<i>c</i>	-10.518030	2836.0715	1582.7028*	651.1945
$S = 0, T = 1(np)$	<i>c</i>	-10.812190	2816.4190	1578.2721*	1002.5300
$S = 0, T = 1(nn)$	<i>c</i>	-10.518030	2832.4903	1580.7610*	651.1945
$S = 0, T = 1$	<i>l2</i>	0.134747	-9.4691	-5.1342*	0
$S = 0, T = 0$	<i>c</i>	-4.739629	1121.2225	466.8222*	2764.3395
	<i>l2</i>	-0.227084	166.5629	90.3117*	0
$S = 1, T = 1(pp)$	<i>c</i>	-9.882847	2589.7742	1389.2081*	2952.3910
$S = 1, T = 1(np)$	<i>c</i>	-9.882847	2587.9836	1386.1622*	2952.3910
$S = 1, T = 1(nn)$	<i>c</i>	-9.882847	2586.1930	1387.2664*	2952.3910
$S = 1, T = 1$	<i>l2</i>	-0.008159	132.7694	71.9886*	-169.8510
	<i>t</i>	1.420069	0	-453.5357	-837.3820
	<i>ls</i>	-1.749197	-493.8470	-267.7677*	1533.0637
	<i>q</i>	0.135181	-17.7975	-9.6499*	-46.2542
$S = 1, T = 0$	<i>c</i>	-8.351808	2325.5929	1307.9923*	957.8091
	<i>l2</i>	-0.023577	1.8164	0.9849*	127.2921
	<i>t</i>	1.327862	0	-1170.8528	580.5596
	<i>ls</i>	0.060223	58.3208	31.6220*	-126.0235
	<i>q</i>	0.000589	-25.1123	-13.6161*	-4.6897

TABLE II: RMS deviations of pp phases in degrees for AV18pq compared to AV18.

Channel 1-25 50-150 200-350 Total PWA93

	MeV	MeV	MeV		
1S_0	0.021	0.031	0.245	0.149	0.181
1D_2	0.001	0.011	0.061	0.037	0.055
1G_4	0	0.001	0.020	0.012	0.029
3P_0	0.024	0.024	0.092	0.059	0.224
3P_1	0.002	0.035	0.074	0.048	0.109
3P_2	0.008	0.090	0.160	0.107	0.062
ε_2	0.002	0.011	0.044	0.027	0.048
3F_2	0.001	0.013	0.055	0.034	0.062
3F_3	0.002	0.042	0.034	0.030	0.054
3F_4	0.002	0.054	0.077	0.054	0.043
ε_4	0	0.005	0.009	0.006	0.001
3H_4	0	0.018	0.047	0.030	0

 TABLE III: RMS deviations of np phases in degrees for AV18pq compared to AV18.

Channel 1-25 50-150 200-350 Total PWA93

	MeV	MeV	MeV		
1S_0	0.018	0.087	0.078	0.067	0.344
1P_1	0.005	0.029	0.064	0.041	0.160
1F_3	0	0.003	0.022	0.013	0.047
3S_1	0.095	0.113	0.387	0.248	0.154
ε_1	0.011	0.061	0.048	0.043	0.115
3D_1	0.002	0.086	0.200	0.129	0.127
3D_2	0	0.037	0.139	0.086	0.090
3D_3	0.001	0.017	0.230	0.139	0.069
ε_3	0.001	0.005	0.036	0.022	0.035
3G_3	0	0.001	0.004	0.002	0.002
3G_4	0	0.027	0.253	0.153	0

TABLE IV: Comparison of static deuteron properties and expectation values for different terms in the potentials.

	Expt	AV18q	AV18pq	
E_d	2.224575(9)	2.224575	2.224573	MeV
$\langle T \rangle$		19.810	19.525	MeV
$\langle V \rangle$		-22.035	-21.750	MeV
$\langle v^c \rangle$		-4.446	-4.079	MeV
$\langle v^t \rangle$		-16.586	-17.462	MeV
$\langle v^{ls} \rangle$		-0.690	-0.313	MeV
$\langle v^{l2} \rangle$		1.087		MeV
$\langle v^{p2} \rangle$			1.440	MeV
$\langle v^q \rangle$		-1.418	-1.354	MeV
$\langle v^{EM} \rangle$		0.018	0.018	MeV
A_S	0.8781(44)	0.8850	0.8863	$\text{fm}^{1/2}$
η	0.0256(4)	0.0250	0.0250	
r_d	1.953(3)	1.967	1.969	fm
μ_d	0.857406(1)	0.847	0.847	μ_0
Q_d	0.2859(3)	0.270	0.270	fm^2
P_d		5.76	5.78	%

TABLE V: Binding energies of light nuclei (in MeV) for different Hamiltonians as computed by the variational Monte Carlo (VMC) method, with comparisons to relevant Green's function Monte Carlo (GFMC) results of Ref. [7] and Faddeev-Yakubovsky (FY) results of Ref. [18]. We also show FY results for the Nijmegen potential at the bottom. Different versions of the Tucson-Melbourne (TM) force are characterized by the cutoff parameter Λ shown in parentheses.

Hamiltonian	Method	^3H	^3He	^4He
AV18	VMC	−7.50(1)	−6.77(1)	−23.70(2)
	GFMC	−7.61(1)	−6.87(1)	−24.07(4)
	FY	−7.623	−6.924	−24.28
AV18pq	VMC	−7.50(1)	−6.77(1)	−23.79(2)
AV8'	VMC	−7.65(1)	−7.01(1)	−24.69(2)
	GFMC	−7.76(1)	−7.12(1)	−25.14(2)
AV18/UIX	VMC	−8.29(1)	−7.53(1)	−27.58(2)
	GFMC	−8.46(1)	−7.71(1)	−28.33(2)
	FY	−8.478	−7.760	−28.50
AV18pq/UIX	VMC	−8.22(1)	−7.47(1)	−27.21(2)
AV8'/UIX	VMC	−8.51(1)	−7.86(1)	−29.05(2)
	GFMC	−8.68(1)	−8.03(1)	−29.82(2)
AV18/TM'(4.756)	VMC	−8.26(1)	−7.50(1)	−27.51(2)
	FY	−8.444	−7.728	−28.36
AV18pq/TM'(4.756)	VMC	−8.22(1)	−7.46(1)	−27.42(2)
AV8'/TM'(4.756)	VMC	−8.44(1)	−7.79(1)	−28.83(2)
Nijm I	FY	−7.736	−7.085	−24.98
	FY	−7.654	−7.012	−24.56
	FY	−8.392	−7.720	−28.60
	FY	−8.386	−7.720	−28.54

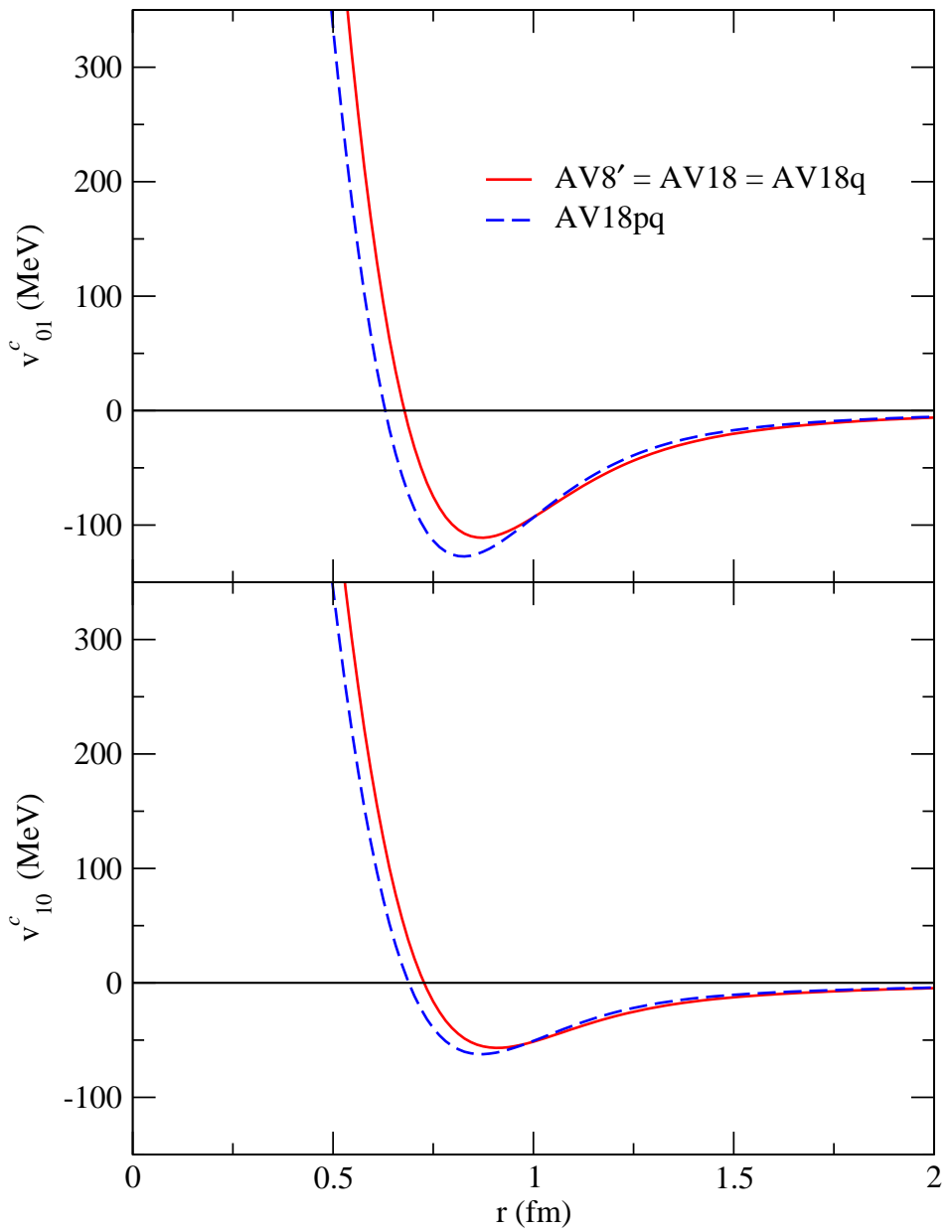


FIG. 1: (Color online) Central potentials in even-parity waves.

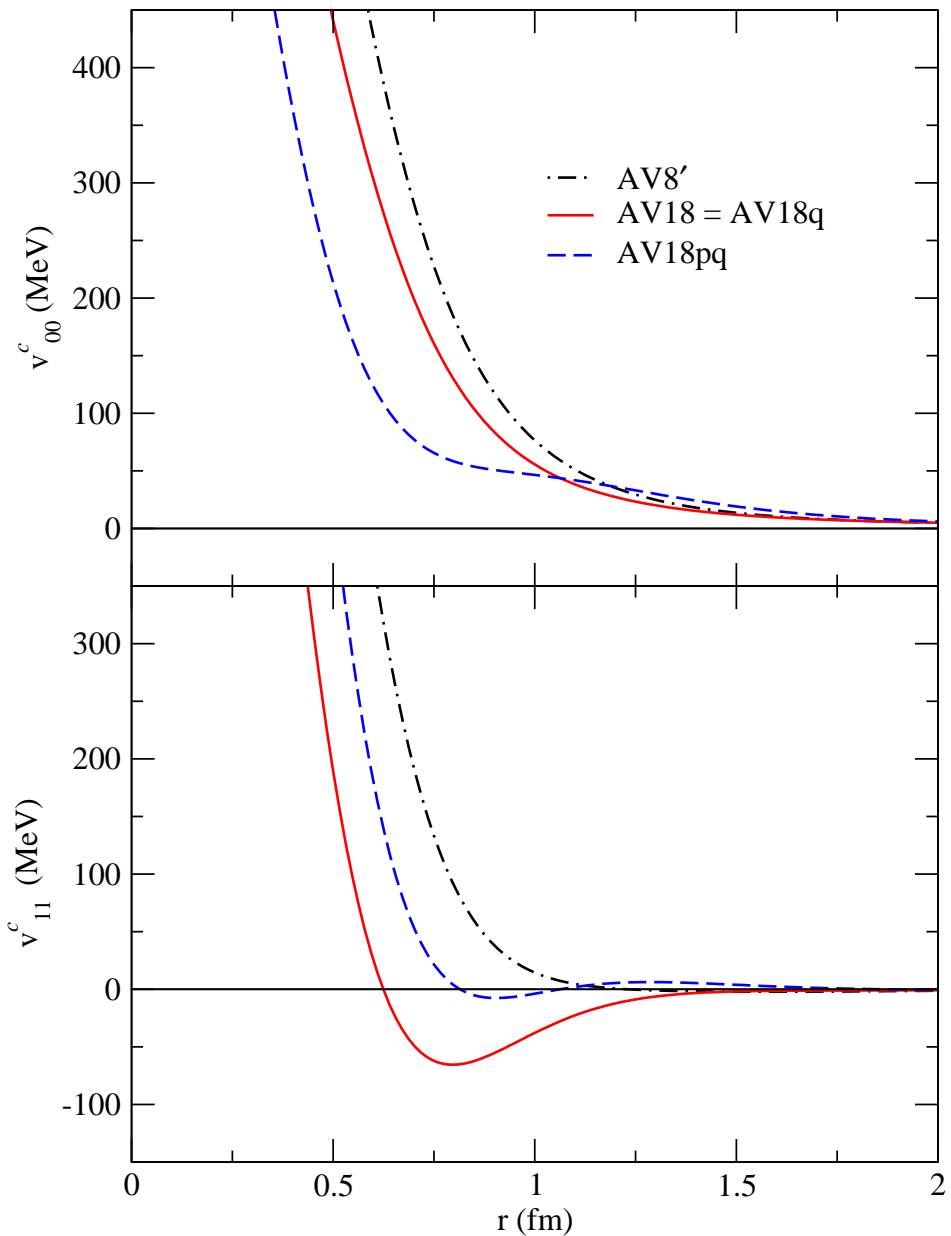


FIG. 2: (Color online) Central potentials in odd-parity waves.

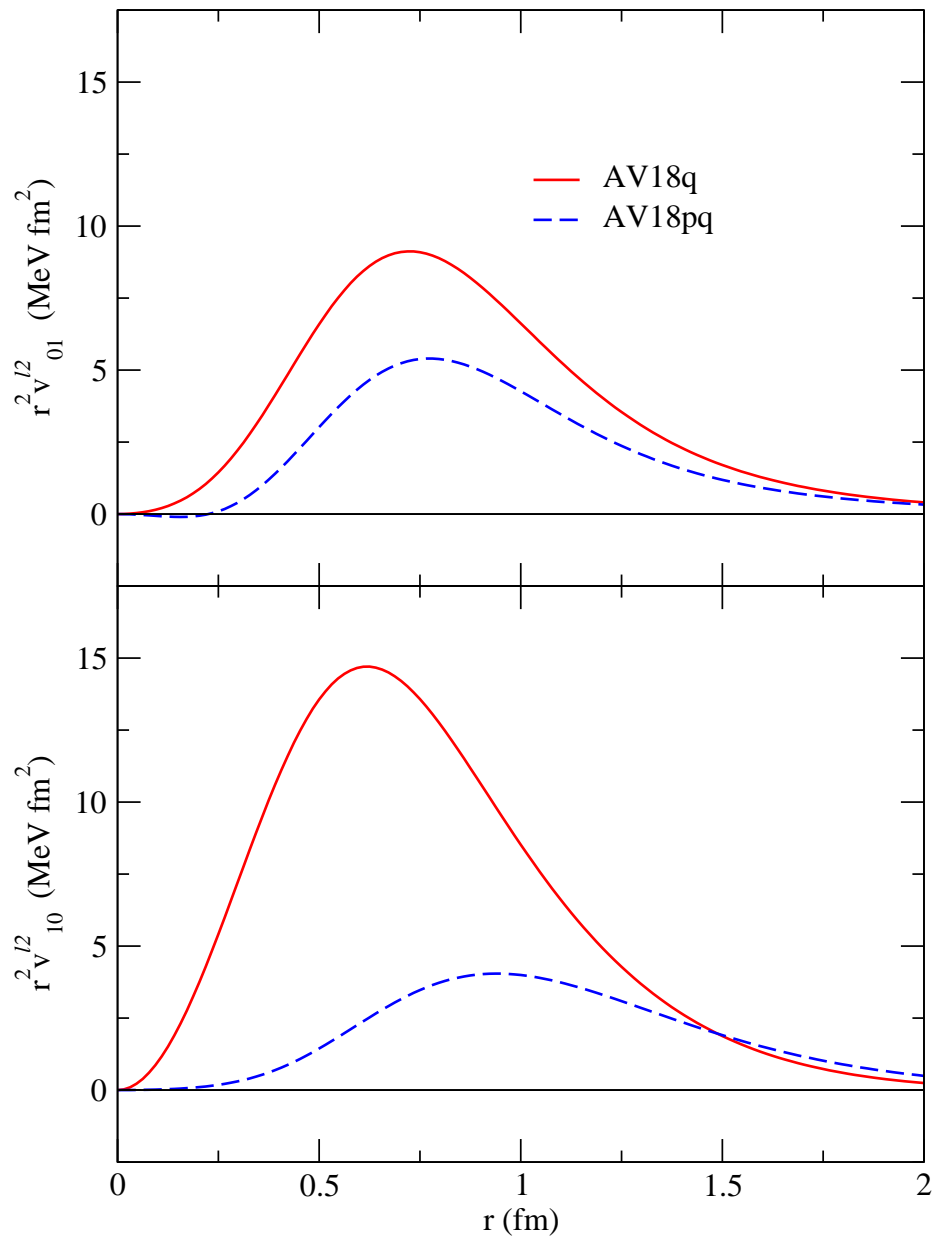


FIG. 3: (Color online) Quadratic momentum-dependent potentials in even-parity waves.

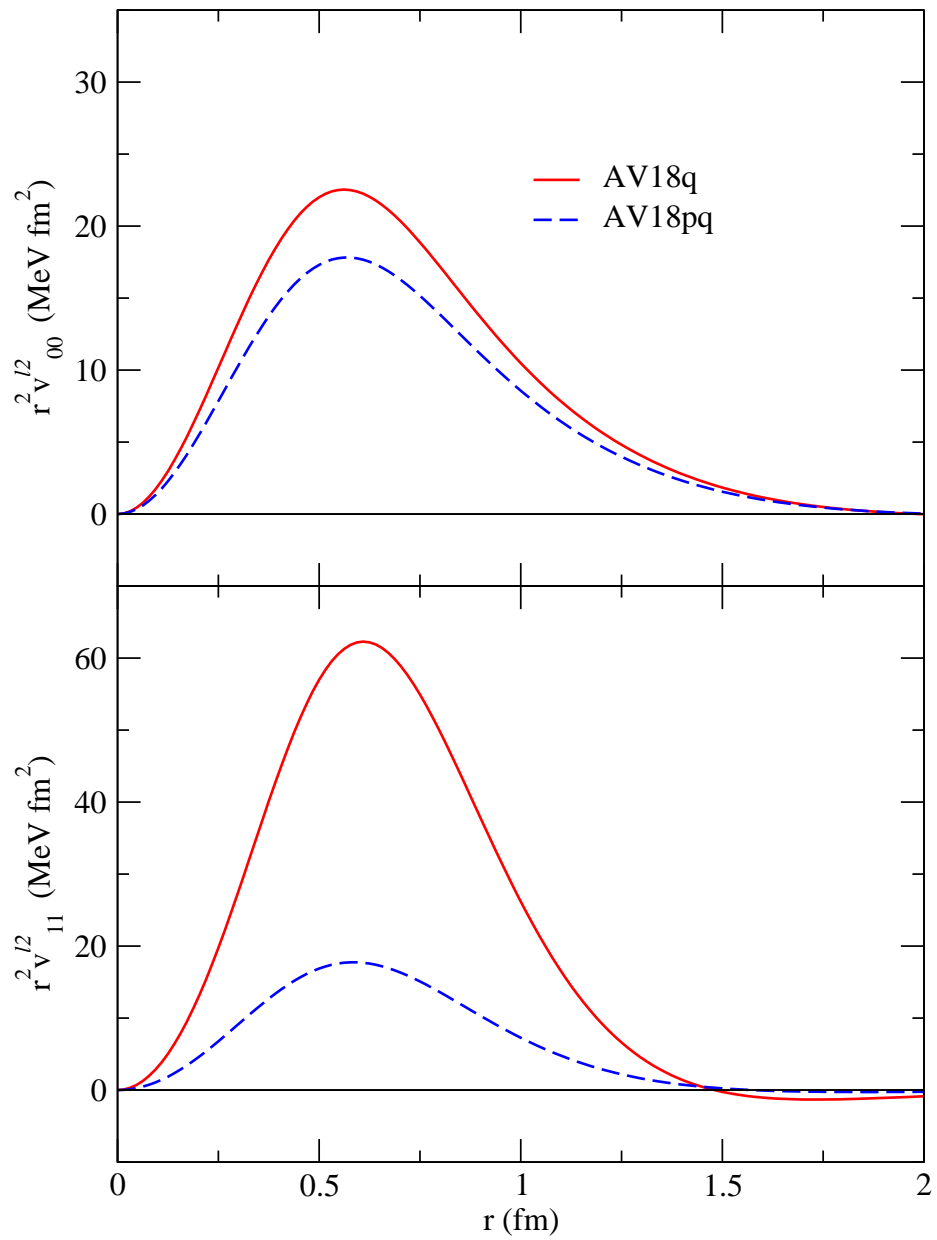


FIG. 4: (Color online) Quadratic momentum-dependent potentials in odd-parity waves.

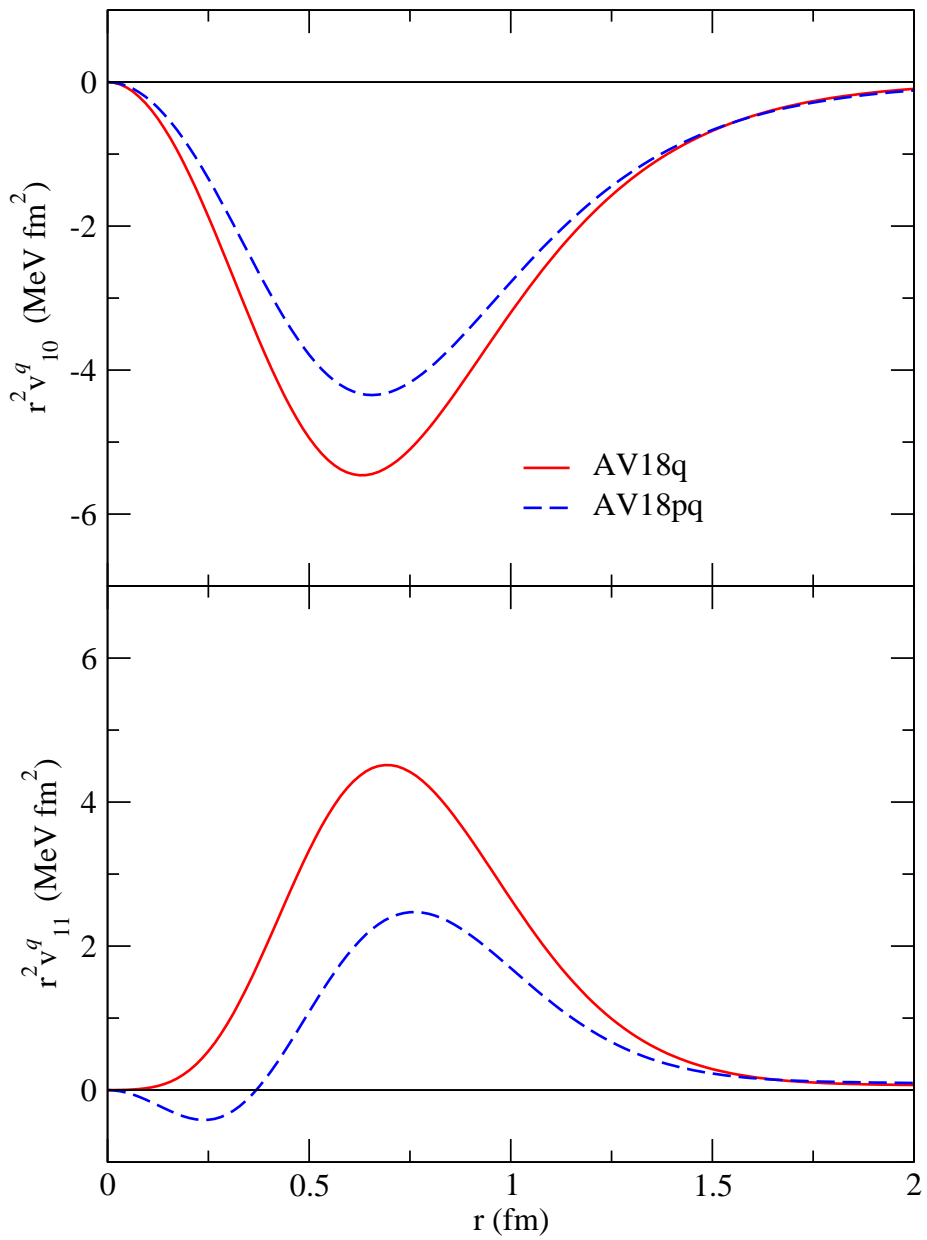


FIG. 5: (Color online) Quadratic spin-orbit potentials in $S = 1$ channels.

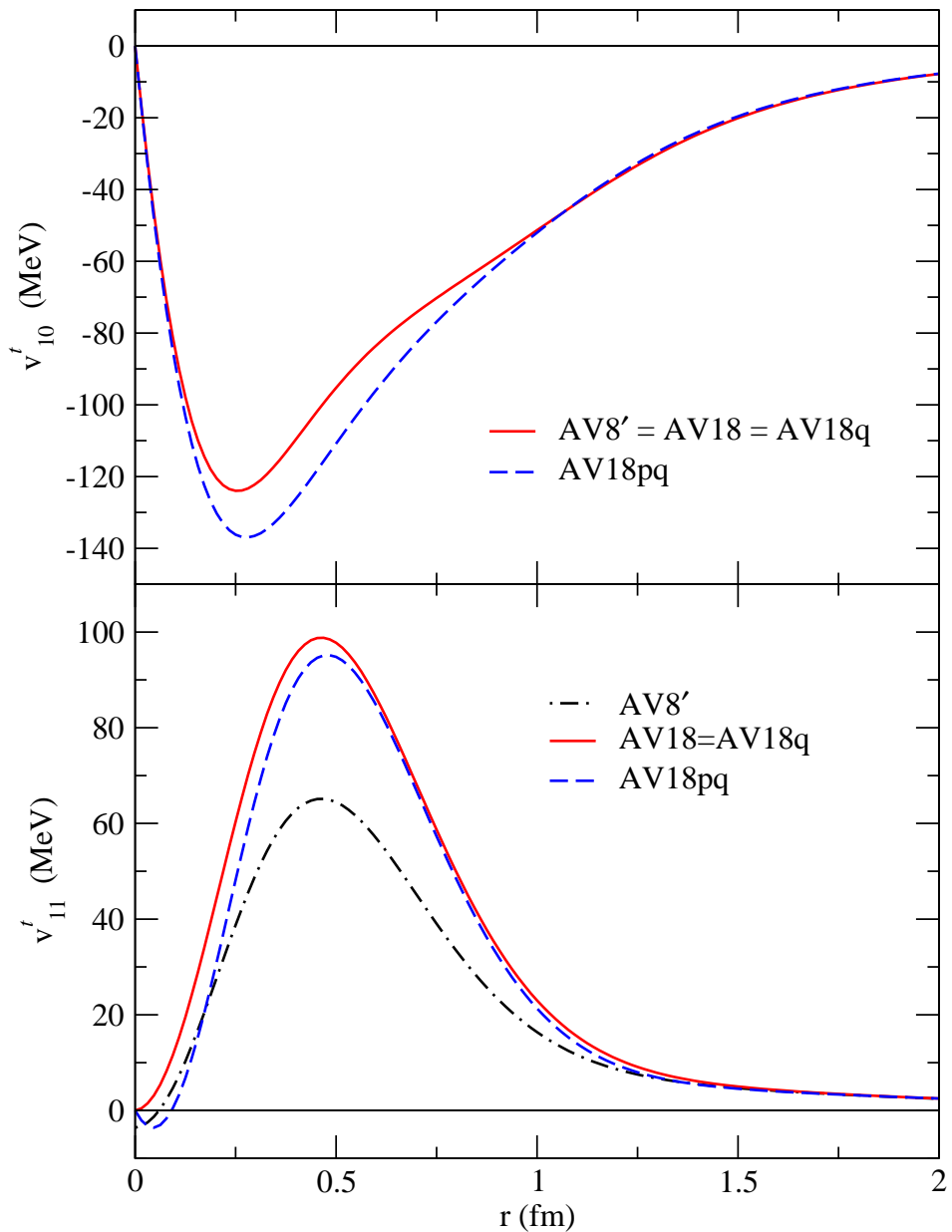


FIG. 6: (Color online) Tensor potentials in $S = 1$ channels.

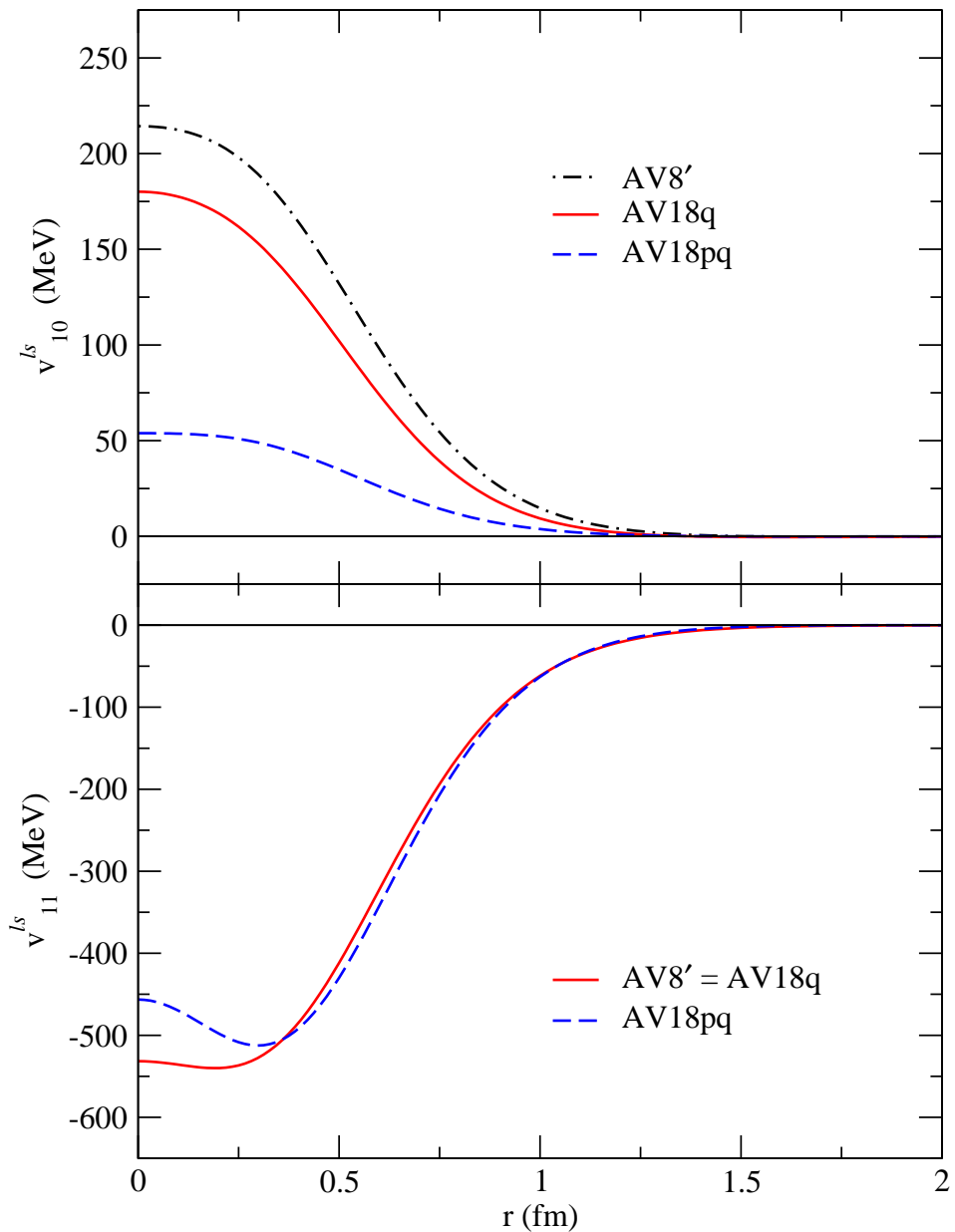


FIG. 7: (Color online) Spin-orbit potentials in $S = 1$ channels.

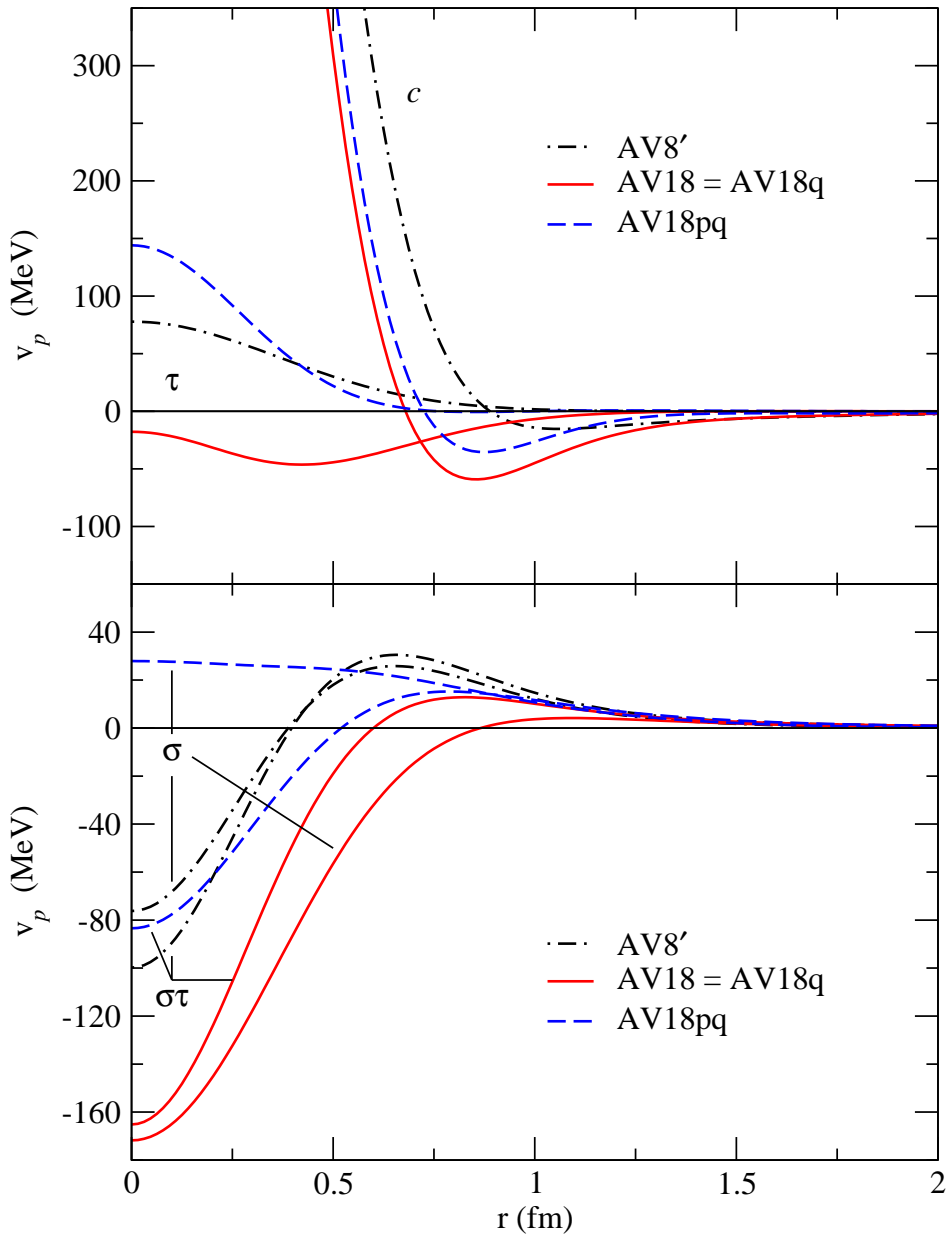


FIG. 8: (Color online) The $v_{p=1,4}$ projected from the v_{ST}^c .

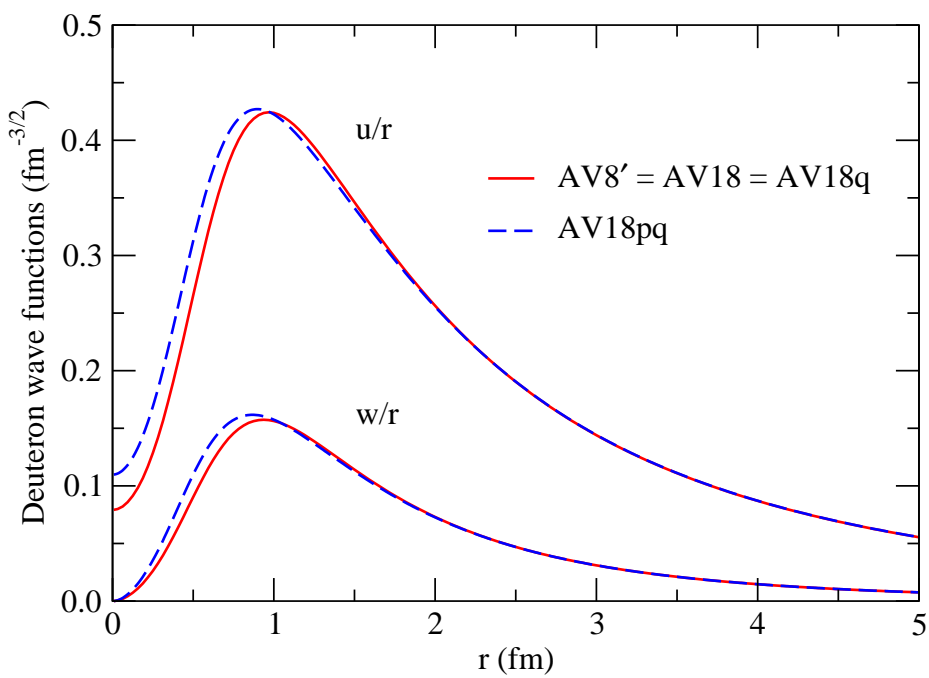


FIG. 9: (Color online) Deuteron S - and D -wave functions.

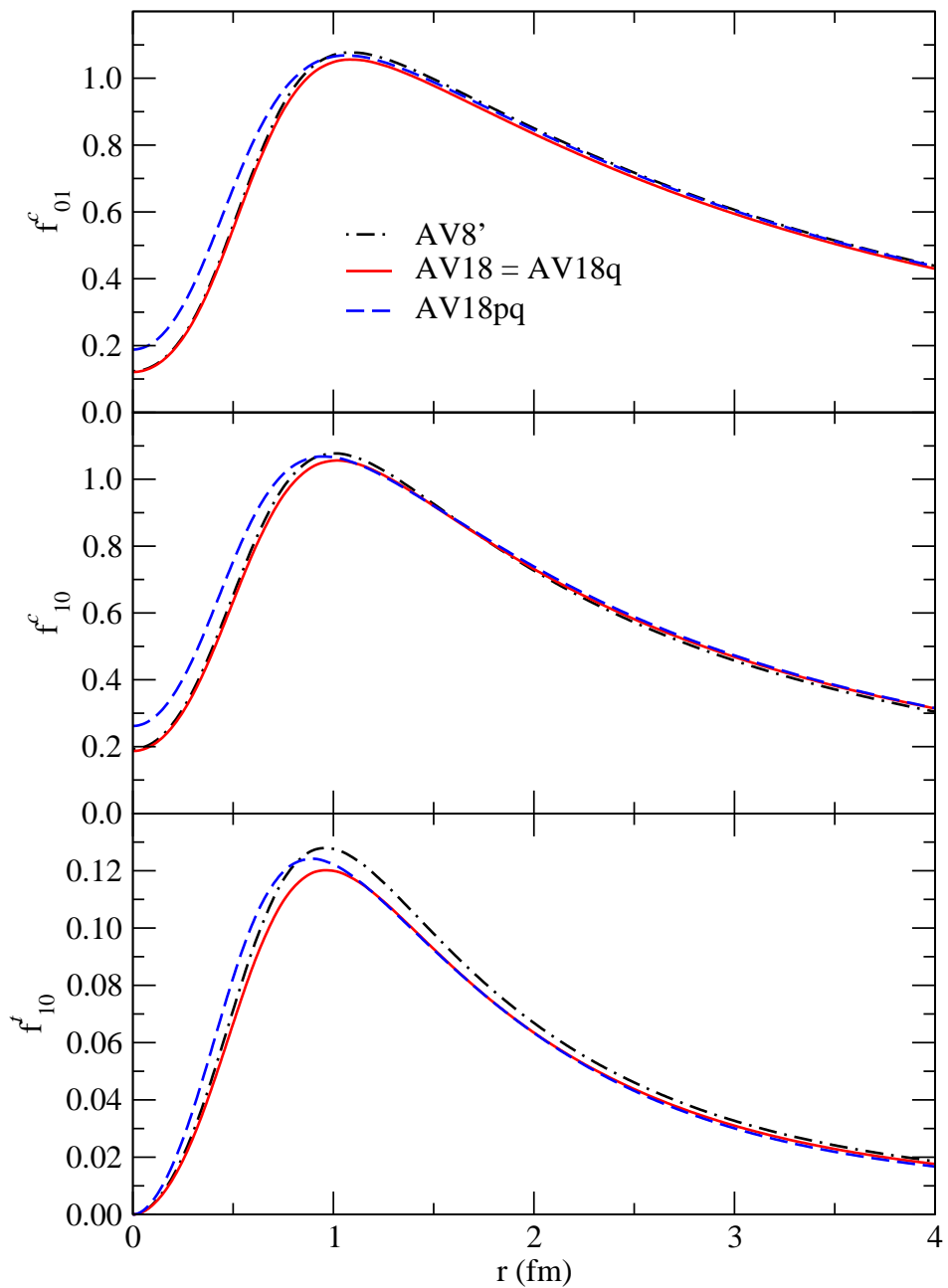


FIG. 10: (Color online) Correlation functions for S -wave channels in ${}^4\text{He}$.